Laser induced microexplosions of a photosensitive polymer

L.S. Bennett[1], T. Lippert[2], H. Furutani[3,*], H. Fukumura[3], H. Masuhara[3,*]

[1] National Institute of Materials and Chemical Research, Tsukuba, 305, Japan
[2] Los Alamos National Laboratory, Los Alamos, NM, 87545, USA
[3] Department of Applied Physics, Osaka University, Suita, Osaka 565, Japan
(Fax: + 81-6/876-8580, E-mail: fukumura@ap.eng.osaka-u.ac.jp)

Abstract. Laser ablation of a photosensitive triazene polymer was studied in a micro region by means of a nanosecond imaging technique. The propagation of a blast wave, 100 ns after laser irradiation, sufficiently matched a planar blast wave model including the decomposed source mass which indicates characteristics of a microexplosion. The measured velocities of the fronts indicates two blast waves: an initially fast unsupported wave around the peak of the laser pulse, and a relatively slow supported wave involving the main component of the decomposition.

PACS: 42.10; 78.65; 81.60.Z; 82.40.Z

Laser ablation is one promising method for fabricating microstructures. In particular, the use of laser ablation in material processing has been expanding considerably in the field of microelectronics [1]. Under well-controlled conditions, a pulsed UV laser can instantaneously cut, bore or etch some polymeric materials, leaving clean contours and sharp edges. Most cases are, however, not free from problems of solid debris remaining at the surfaces. This has been considered to be caused by the ejection of incompletely decomposed materials and their re-adhesion onto the surface. To avoid this kind of contamination in microfabrication, an understanding of how materials are decomposed and ejected is necessary.

In this report, a photodecomposable polymer which is known to be a good material for high-resolution microlithography [2, 3] was used to study the dynamics of the ejected plume near the surface by a nanosecond imaging technique. The ejected plume has been compared to a microexplosion producing shock waves in the surrounding gaseous media which have been used to classify the explosion and discuss the energy released [4–6]. The shock waves observed resemble explosively formed blast waves which can be analyzed with point blast theory or may necessitate the use of a theory that includes the source mass of the explosion close to the polymer surface.

*To whom all correspondence should be addressed.

1 Blast waves

In a spherical explosion that forms a blast wave, the reaction is assumed to occur instantaneously, and the energy released by the explosion, E_0, is mainly deposited in the gaseous product. This high-pressure gas expands at a velocity greater than the speed of sound in the surrounding atmosphere and acts as a piston pushing this atmosphere outward in a compressive wave referred to as a blast wave. This wave travels faster than the product front and encompasses an ever-increasing spherical volume of the surrounding atmosphere. Because the energy supplied by the explosion is finite, the blast wave strength polynomially decays with radial propagation distance.

The rate of the blast wave propagation is used to classify it as either a weak, intermediate or strong blast wave. A weak blast wave travels near to the speed of sound in the surrounding atmosphere [6]. The propagation of a strong blast wave may be analyzed with a few simplifying assumptions concerning the explosive such as its energy being instantaneously released into the gaseous product, a negligible point mass source of this energy and a spherical shock occurring in the surrounding atmosphere. With these assumptions, the propagation radius, R, and time, t, may be related for a strong blast wave [6–8],

$$R = \xi_0 (E_0/\rho_0)^{1/5} t^{2/5}, \tag{1}$$

where ρ_0 is the undisturbed atmospheric density and the constant, ξ_0, may be found from strong shock theory [8].

The negligible explosive mass assumption leads to this being referred to as a "point blast theory" and imposes limitations on the propagation radius to which (1) applies. A minimum radius limitation, R_1, is determined by the mass of the atmosphere encompassed by the spherical blast wave being significantly greater than the original explosive mass, M_0. In the case of excimer-laser-induced reactions on a polymer plate, the plate and its backing will act as a boundary, so the mass encompassed by the blast wave is only a hemisphere, $2/3\pi\rho_0 R^3$, thus R_1 should be

328

expressed as [5],

$$R_1 = \left(\frac{3M_0}{2\pi\rho_0}\right)^{1/3}. \tag{2}$$

The propagation distance must be about an order of magnitude greater than R_1 for (1) to apply, but it may suffice to use only a multiple of five [5].

The maximum radius limitation, R_2 occurs when the peak pressure within the blast wave, P_1, is no longer significantly greater than that ahead of it in the ambient atmosphere, P_0. When $P_1 \cong P_0$, strong shock relations no longer apply. This limit has been estimated to occur at the radius where a sphere containing ambient atmosphere has an equal internal energy to the energy of the explosion [5],

$$R_2 \cong (E_0/P_0)^{1/3}. \tag{3}$$

For a blast wave propagation radius less than the minimum radius, models that do not neglect the mass of the explosion product should be applied. Two analytical solutions that include the source mass are readily available in the strong shock regime. In formulating both of these, the effects of shock waves in the relatively thin polymer and quartz backing are ignored. Since the shock speeds in the solid materials are significantly faster than those in the surrounding air, the effects of the shock waves through these materials will terminate within the first few nanoseconds.

The first analytical solution applies to planar blast waves which will be the case at the center of the laser irradiation area for a limited propagation radius until the edge effects converge on the center axis [9]. Several assumptions are necessary in this theory, such as one-dimensional, instantaneous transfer of the explosive energy into the product gases, uniform distribution of the compressed atmosphere behind the blast front and averaging of the explosive product velocity and pressure [9]. Applying hydrodynamic conservation laws along with these assumptions allows a solution for the propagation radius with respect to the propagation time,

$$R = \{[1.5\,C_5(E_0)^{1/5}\,t + C_4^{3/2}]^{2/3} - C_4\}/C_5, \tag{4}$$

where

$$C_4 = \frac{A\delta}{8}\left(\frac{2}{\gamma+1}\right)^2\rho_s \qquad C_5 = \frac{\rho_0 A}{\gamma+1}\left(\frac{1}{\gamma-1}+\frac{4}{\gamma+1}\right).$$

Here, γ is the specific heat ratio of the atmosphere, A is the planar area, ρ_s is the initial explosive density and δ is the axial thickness of the explosive prior to detonation. In the laser-induced ablation case, these will be the laser-ablated area, the solid polymer density and the ablation depth, respectively.

The second analytical solution that includes the explosive mass applies to a spherical blast wave [8]. Again, several assumptions are used, such as instantaneous transfer of the explosive energy to a spherical mass of expanding product gases, averaging the mass of the product gases over its radius and uniform distribution of the compressed atmosphere into an isotropic spherical shell [8]. These assumptions along with flow conservation laws allow a solution for the propagation radius in the form of

a differential equation,

$$\frac{dR}{dt} = \left[\frac{E_0}{C_1 + C_2 R^3}\right]^{1/2}, \tag{5}$$

where

$$C_1 = \frac{4\pi}{3(\gamma+1)^2}\rho_s R_s^3 \qquad C_2 = \frac{4\pi\rho_0}{3}\left(\frac{2}{(\gamma+1)^2}+\frac{1}{(\gamma^2-1)}\right).$$

Here, R_s is the initial radius of the hemispherical explosive charge and the constants C_1 and C_2 reflect the volumes encompassed by a hemispherical blast wave instead of the spherical blasts for which the solution was initially designed. Although the original authors of this formulation choose to evaluate (5) in terms of an elliptic integral [8], a simple computational solution utilizing a fourth-order Runge-Kutta method was employed here.

2 Experimental

In this investigation, a photosensitive triazene polymer with the structure shown in Scheme 1 was prepared by a previously reported method [10]. The polymer was dissolved in tetrahydrofuran and spin coated on quartz plates to a thickness of ca. 1 μm. The films were cured for more than 24 h at 50 °C to remove the residual solvent. The beam from a XeF excimer laser (Lambda Physik, LEXTRA 200, 351 nm, fwhm 20 ns) was focused into a small spot, 1.63×1.24 mm square, on the surface of the sample film to induce a microexplosion. Ejected plumes and blast waves were illuminated by fluorescence from a methanol solution of Rhodamin 101 which was excited by the second harmonic of a Q-switched Nd^{3+}:YAG laser (Continuum Surelite, fwhm 10 ns). The resulting images, recorded by a synchronously operated CCD camera, appear similar to shadowgraphs. The delay between the two lasers was adjusted by a digital pulse generator. The principles of this imaging method are the same as those reported previously for poly(methylmethacrylate) (PMMA) [11–14] and liquid benzene [15].

The majority of a series of shadowgraphs recorded at a laser fluence of 50 mJ/cm² are displayed in Fig. 1 and most of those from a series of experiments with a 250 mJ/cm² fluence laser are shown in Fig. 2. The time zero chosen for these photographs was at the peak of the excimer laser irradiation [16]. In this time zero reference, a photo was also taken at time $= -4.8$ ns for the 50 mJ/cm² fluence laser and at time $= -7.2$ ns for the 250 mJ/cm² fluence laser. Although both of these 'negative' time photos were well after the beginning of the laser irradiation, neither showed any indication of shock wave

Scheme 1.

329
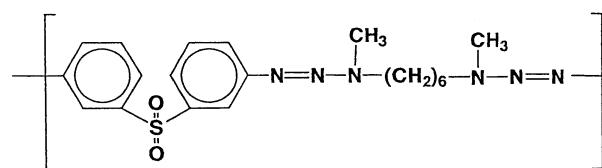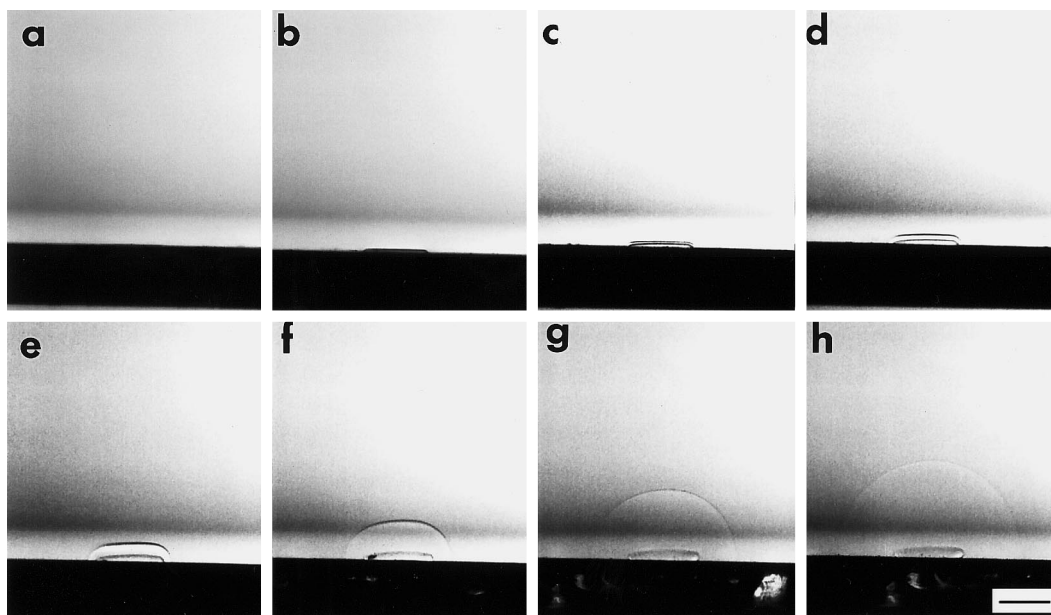
Fig. 1. A series of nanosecond shadowgraphs showing the shock fronts formed in the 50 mJ/cm² fluence case. Delay time; **a** − 4.8 ns; **b** 51.2 ns; **c** 106 ns, **d** 200 ns; **e** 420 ns; **f** 1000 ns; **g** 2000 ns; **h** 3000 ns. The *bar* indicates 1 mm on this scale
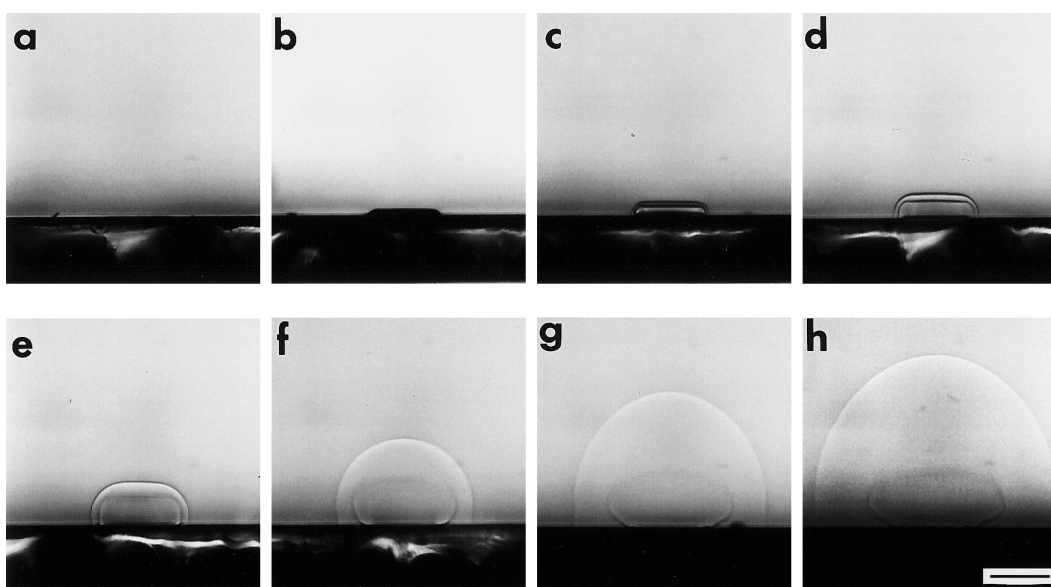
Fig. 2. A series of nanosecond shadowgraphs showing the shock fronts formed in the 250 mJ/cm² fluence case. Delay time; **a** − 7.2 ns; **b** 44.8 ns; **c** 111 ns; **d** 204 ns; **(e)** 407 ns; **f** 1000 ns; **g** 2000 ns, **h** 3000 ns. The *bar* indicates 1 mm on this scale

formation or material expansion [14]. A depth profiler (Sloan, Dektak II) was used to measure a final ablation depth of 50 nm in one of the 50 mJ/cm² fluence case experiments and 650 nm in one of the 250 mJ/cm² fluence case experiments.

3 Analysis

To analyze these experiments, the blast wave was first classified by plotting the measured blast wave propaga-tion distance in each photo vs. time on a log-log plot. The slope of this log-log plot will simply be the time dependency constant and thus determine the blast wave strength. A weak blast wave will have a slope of 1.0 and a strong blast wave will have a slope of 0.4 on this type of plot.

The propagation distances were measured in reference to the initial surface at the center of the ablated area in each photo. As will be further discussed, the photos showing shock waves before 100 ns in each fluence strength series should be treated separately from this blast wave portion of the analysis. For the 50 mJ/cm² fluence laser

case, the remaining photos from Fig. 1 were divided into sequential sets to show the time dependency constant develops from an initial value of 0.87 to a final value of 0.80. For the 250 mJ/cm^2 fluence laser, the later series of photos from Fig. 2 show that the time dependency constant develops from an initial value of 0.83 to a final value of 0.64.

The minimum radius, R_1, for which a point source solution applies was calculated from (2) where the mass of the 'exploded' polymer was found from the volume ablated and the density of the polymer, $\rho_s = 1.2$ g/cm^3. These measured volumes, V, the mass they represent, M_0, and the calculated values of the minimum radius are listed in Table 1 for both fluence cases. Since the ablation depth was measured for only one of the series of experiments in each fluence case, the ablated volume and mass may be a source of error when comparing these calculations to the measured values.

The majority of the measurements in Figs. 1 and 2 are within an order of magnitude of the minimum radii, so the theories including explosive mass should be applied. Thus, the log-log slopes of greater than 0.4 do not necessarily indicate that the blast waves are below the strong shock regime, but that they may simply still be influenced by the mass of the microexplosion product.

For laser-induced ablation of polymers, the energy released by the chemical reaction and the volumetric expansion does not seem sufficient to produce a self-propagating detonation in the polymer. As a result, the energy released by the reaction in (1)–(5) is often neglected and just the laser irradiation energy, E_{is}, or some fraction of this is substituted for E_0 [4, 5, 16, 17]. Experiments in which metallic plates were ablated with a pulse laser displayed good agreement with (1) given this substitution [16, 17]. Beh-Eliahan et al. [6] included the energy released by the thermal decomposition, E_{th}, of their glycidyl azidopolymer in addition to the laser irradiation energy.

These energy values will be influenced by the area irradiated and the volume of polymer ablated, which are listed in Table 1. The decomposition enthalpy of the polymer has previously been measured as -258 kJ/mol and the molecular weight is 413.8 g/mol [2]. Thus, the decomposition-specific enthalpy is -623.5 J/g. A common assumption in models of energetic reactions is that the decomposition-specific energy is equal to the decomposition-specific enthalpy at atmospheric pressure

[18]. Assuming all of the decomposition energy is released by the ablated mass, allows the decomposition energy, E_{th}, to be found by multiplying this specific energy by the ablated mass. The decomposition energy and the total laser energy, E_{is}, i.e. the fluence multiplied by the irradiated area, are also listed in Table 1. The shocks will be propagating through air initially at about ambient pressure and temperature which has a density of 1.1844×10^{-3} g/cm^3 and a specific heat ratio, γ, of 1.4.

Utilizing the values given in Table 1, a study of the energy deposited into the product gases was conducted with the planar and spherical models, (4) and (5), for the blast wave propagation distance. The amount of laser energy deposited in the polymer should decay exponentially with the penetration depth. The absorption coefficient for this polymer with a 351-nm excimer laser has been measured as 4.56/μm. From this coefficient it is calculated that only 5.1% of the energy should be absorbed by the first 50 nm of material as in the 50 mJ/cm^2 fluence case and 99.8% should be absorbed in the 650 nm ablated in the 250 mJ/cm^2 case. However, the best fits to the measured blast wave propagation distances were obtained when the maximum available energy was employed, i.e. 100% of the laser irradiation energy and the thermal decomposition energy, for both fluence cases. This may be reasonable since the absorbance increases beyond the ablation threshold fluence [19–22].

A comparison of the measured blast wave propagation distances to those calculated by (4) and (5) using the either just the laser energy, E_{is}, or the maximum available energy, $E_{is} + E_{th}$, is shown in Fig. 3. For both fluence cases the planar model with the maximum available energy produces the best agreement with the measured data. This agreement is not surprising within the first few hundred nanoseconds since the edge effects should not have interfered with the planar region in this time, but this is not expected after the edge effects have converged on the center axis. The encroachment of the edge effects is apparent in Figs. 1 and 2 which show the flat tops of the blast waves decreasing with time.

For the spherical model, it was necessary to calculate the radius of an initially hemispherical polymer mass, R_s, based on the volume of the ablated slab, $V = A\delta$, as a starting point for the numerical integration of (5). These radii are given in Table 1. The failure of the spherical model to sufficiently fit the measured data is not surprising, because the minimum width of the ablated area is of the same order of magnitude as the propagation distance.

The blast wave and product front velocities, U_i, may be found by measuring the distance travelled between each sequential set of photographs, $\Delta R_i = R_i - R_{i-1}$, based on the distance from the initial polymer surface and dividing this by the time elapsed between each photo, Δt_i, i.e. $U_i = \Delta R_i / \Delta t_i$. This method yields only the average velocity between each sequential set of photographs and not the instantaneous velocity of each. These calculated velocities are plotted vs. time for both the 50 mJ/cm^2 and the 250 mJ/cm^2 fluence cases in Fig. 4. Since each photo was taken from an independent experiment, these measured velocities may contain significant error. However, the general trends discussed below seem to be the same and indicate similar phenomena in both fluence cases.

Table 1 Values used to calculate the blast wave propagation distance

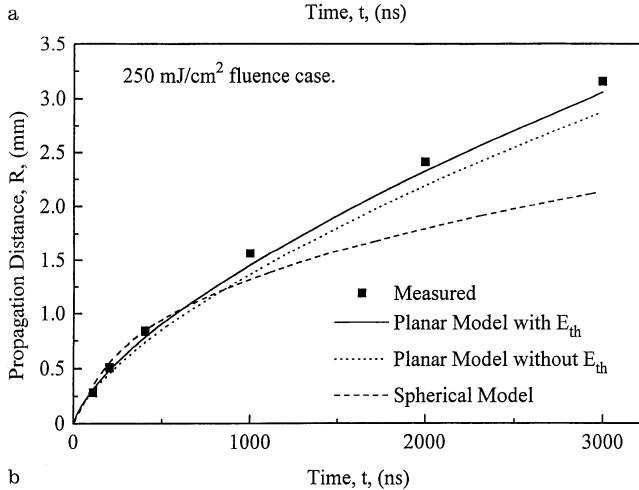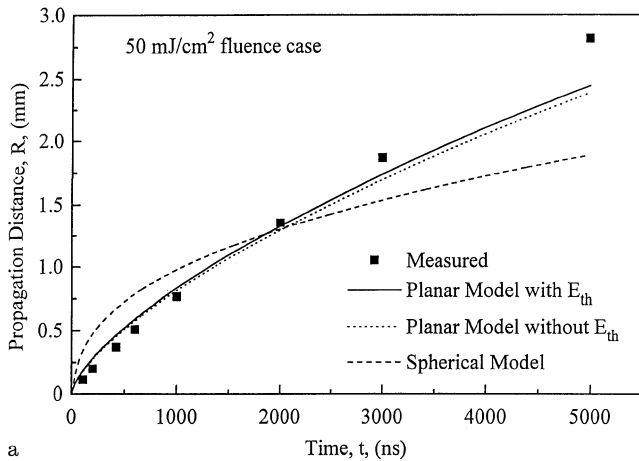|	50 mJ/cm^2	250 mJ/cm^2
Ablated volume, V, (mm^3)	1.011×10^{-4}	1.314×10^{-3}
Ablated mass, M_0, (g)	1.213×10^{-7}	1.577×10^{-6}
Irradiated area, A, (mm^2)	2.021	2.012
Minimum radius, R_1, (mm)	0.366	0.860
Maximum radius, R_2, (mm)	2.205	3.906
Laser energy, E_{is}, (mJ)	1.011	5.053
Thermal decomposition energy, E_{th}, (mJ)	0.076	0.983
Equilivent hemispherical radius, R_s, (mm)	0.036	0.086

Fig. 3. Measured and calculated blast wave propagation distances by planar and spherical models including the source mass

Fig. 4. Initial shock and blast wave velocities and product front velocities

For both fluences, only one front was visible until about 100 ns, after which two fronts became distinguishable. As can be seen in Fig. 4a and b, the velocity of this initial shock wave rapidly decays well below the velocity at which the blast wave next appears. This leads to the conclusion that this initial shock is separate from the blast wave or product front. Therefore, the first velocities calculated for both the blast wave and product front in both the 50 and 250 mJ/cm² fluence laser can be questioned, since they are based on the final position of the initial shock. Because of this doubt, these points have been left open in contrast to the filled points used for the remainder of the blast wave and product front points.

The apparently separate initial shock is of particular interest, because it appears in both fluence cases and persists for a similar duration even though the propagation distance is quite different. This indicates that a relatively strong material ejection occurs near the peak of the laser pulse and then abruptly stops. In both fluence cases this initial ejection is followed by the later product front and blast wave structure. The initiation time of the second plume is difficult to specify because it is masked by the first plume, but it seems to be delayed by approximately 100 ns after the first 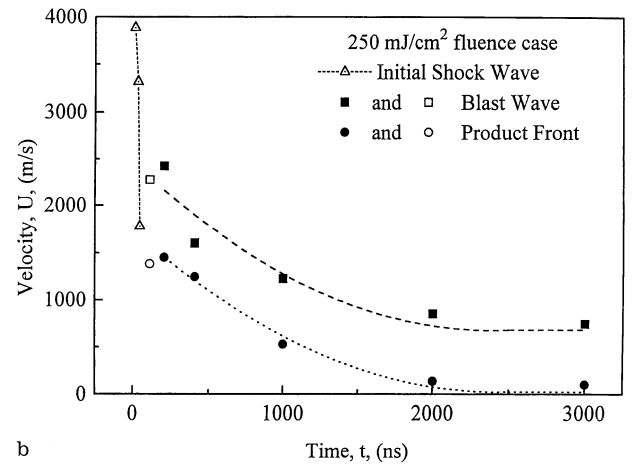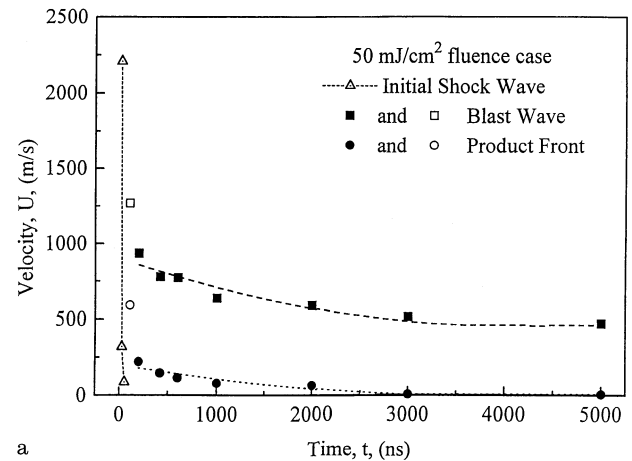ejection. It is possible that these material ejections are the result of either two separate, sequential or independent chemical reactions or the same unstable reaction of the polymer that initiates and quenches and then again re-initiates.

4 Conclusions

For both the 50 and 250 mJ/cm² laser fluence cases, the blast wave propagation distances observed are within an order of magnitude of the minimum propagation radius for a point blast theory. Thus, the blast waves are still developing during these observations as is also indicated by the changing time dependency constant, so any calculations of the blast wave propagation distance must include the mass of the ablated polymer. Of the two source mass theories applied, the one-dimensional approach including all of the laser and thermal decomposition energy best fits to the experimental data for both fluence cases. The front velocity measurements indicate that both cases display an initial shock which seems separate from the later blast wave and product front structure. This dual shock structure may indicate either instabilities in the chemical reaction that forms the ejected product material, or two sequential or independent reactions.

332

References

1. H. Masuhara, A. Itaya, H. Fukumura, *ACS Symposium Series* 412: *Polymers in Microlithography, Materials and Processes* (American Chemical Society, Washington, DC, 1989), 400–410
2. T. Lippert, J. Stebani, J. Ihlemann, O. Nuyken, A. Wokaun, *J. Phys. Chem.* **97**, 12296 (1993)
3. T. Lippert, A. Wokaun, J. Stebani, O. Nuyken, J. Ihlemann, *Angew. Makromol. Chem.* **206**, 97 (1993)
4. A. Gupta, B. Braren, K.G. Casey, B.W. Hussey, R. Kelly, *Appl. Phys. Lett.* **59**, 1302 (1991)
5. P.E. Dyer, J. Sidhu, *J. Appl. Phys.* **64**, 4657 (1988)
6. Y. Ben-Eliahu, Y. Haas, S. Welner, *J. Phys. Chem.* **99**, 6010 (1995)
7. V.P. Korobeinikov, *Problems of Point Blast Theory* (Institute of Physics, New York, 1991), 65–116
8. D.A. Freiwald, R.A. Axford, *J. Appl. Phys.* **46**, 1171 (1975)
9. D.A. Freiwald, *J. Appl. Phys.* **43**, 2224 (1972)
10. J. Stebani, O. Nuyken, T. Lippert, A. Wokaun, A. Stasko, *Makromol. Chem. Phys.* **196**, 739 (1995)
11. H. Kim, J.C. Postlewaite, T. Zyung, D.D. Dlott, *J. Appl. Phys.* **64**, 2955 (1988)
12. R. Srinivasan, B. Braren, K.G. Casey, M. Yeh, *Appl. Phys. Lett.* **55**, 2790 (1989)
13. H. Furutani, H. Fukumura, H. Masuhara, *Appl. Phys. Lett.* **65**, 3413 (1994)
14. H. Fukumura, E. Takahashi, H. Masuhara, *J. Phys. Chem.* **99**, 750 (1995)
15. Y. Tsuboi, H. Fukumura, H. Masuhara, *Appl. Phys. Lett.* **64**, 2745 (1994)
16. J.L. Bobin, Y.A. Durand, Ph. P. Langer, G. Tonon, *J. Appl. Phys.* **39**, 4184 (1968)
17. R.B. Hall, *J. Appl. Phys.* **40**, 1941 (1969)
18. L.S. Bennett, Y. Horie, *Shock Waves* **4**, 127 (1994)
19. H. Fukumura, H. Masuhara, *Chem. Phys. Lett.* **221**, 373 (1994)
20. H. Fujiwara, T. Hayashi, H. Fukumura, H. Masuhara, *Appl. Phys. Lett.* **64**, 2451 (1994)
21. H. Fujiwara, Y. Nakajima, H. Fukumura, H. Masuhara, *J. Phys. Chem.* **99**, 11481 (1995)
22. H. Fujiwara, H. Fukumura, H. Masuhara, *J. Phys. Chem.* **99**, 11844 (1995)